Optics and Lasers in Engineering 51 (2013) 348–357

Contents lists available at SciVerse ScienceDirect

Optics and Lasers in Engineering

journal homepage: www.elsevier.com/locate/optlaseng

# 3D surface profile measurement of unsymmetrical microstructure using Fizeau interferometric microscope

Shih-Wei Yang [a,*], Chern-Sheng Lin [b], Shir-Kuan Lin [a]

[a] Institute of Electrical and Control Engineering National Chiao Tung University, Hsinchu, Taiwan
[b] Department of Automatic Control Engineering, Feng Chia University, Taichung, Taiwan

ARTICLE INFO

*Article history:*
Received 11 August 2012
Received in revised form
27 November 2012
Accepted 7 December 2012
Available online 3 January 2013

*Keywords:*
3D surface profile
Unsymmetrical microstructure
Fizeau interferometer
Bezier curve

ABSTRACT

In this paper, an automatic optical inspection system for the 3D surface profile of an unsymmetrical microstructure using Fizeau interferometer was proposed. This non-contact optical inspection system is suitable for measuring the lens sag and 3D surface profile of symmetrical and unsymmetrical microlenses. Referring to the unsymmetrical microlenses as an example, the distribution of the interference fringes is partly dense and partly rare, and is completely different from the equally dense distribution of symmetrical microlenses. Thus, a novel algorithm is proposed to solve the above mentioned problem in this paper, namely, individually determining the darkest points of the dark fringes and the brightest points of the bright fringes, and fitting these discrete points as close curves through the Bezier curve theory. As the contour lines of an unsymmetrical microlens are obtained, the 3D surface profile of the unsymmetrical microlens can be plotted correspondingly. Furthermore, the proposed system has the following advantages due to its non-contact structure. This system is specifically designed for in-line measurements according to the rapid inspection speed; it has no need to coat a reflective layer on the inspected microstructure, thus avoiding damaging the surface structure of the sample.



## 1. Introduction

As present technology continuously pursues miniaturization, such as mobile phones, digital cameras, webcam lens of the notebook PC, etc., lenses must be miniaturized with the reduced volume of the main body. Therefore, a microlens with a radius of 10 μm–2 mm is extensively used. The process of microlens array uses standard semiconductor process technology, such as photolithography, resist processing, and reactive ion etching [1–4]. This wafer-based process technology considers the accuracy degree of the lens profile surface, and determines the accurate location on the microlens array. Manual inspection may lead to different inspection results as the human eye would feel tired and make misjudgments after long hours of work. Therefore, an automatic inspection system is designed in this study that automatically obtains interference images of a symmetrical microlens or an unsymmetrical microlens, according to the principle of Fizeau interferometer and the machine vision techniques [5–9]. The lens sag of a microlens was determined using a self-developed algorithm, and the microlens surface profile contour line was built by computer graphics technology, which is able to rebuild the 3D surface profile of a microlens.

There are many instruments and methods for measuring the surface shape of a microlens, such as AFM [10,11], Stylus Profiler [12,13], and SEM [14,15]. This type of instruments is expensive and the inspection speed is too slow; moreover, such probe-based measurements will slightly scratch the array surface of the microlens. Therefore, in order to show the practicability of this study more effectively, machine vision technology was used to form a non-contact automatic optical inspection platform.

Yamamoto and Yamaguchi used wavelength scanning Fizeau interferometry to measure the body surface profile and the surface profile height of aluminum coated glass surface. Its principle is that the surface profile of the object is measured by changing the interference signal phase [16]. Charriere et al. used digital holographic microscopy to describe the characteristics of a microlens [17], which allowed objects to be measured in a wide range of shapes as the vibration did not require isolation. However, the measurement structure for the surface shape of a microlens was incompatible with the measurement structure of the light characteristics of a microlens, and had to be measured by two instruments. In other words, the measured object had to be moved. Anna et al. used Full-Field Swept Source optical coherence tomography to measure the 3D shape of a microlens [18], which structure adopted a superbright diode illuminant. Then an electronically controlled frequency adjuster implemented a scan conversion of the illuminant frequency, causing a strong light to

* Corresponding author. Tel.: +886 3 5712121x54423.
*E-mail address:* swyang.nctu@msa.hinet.net (S.-W. Yang).

0143-8166/$ - see front matter © 2012 Elsevier Ltd. All rights reserved.
http://dx.doi.org/10.1016/j.optlaseng.2012.12.004

pass through the analyte, enter a Michelson interference structure to form interference, record the interference patterns obtained at different frequencies, and finally, build the amplitude and phase diagram. Quan et al. proposed a non-contact optical inspection system using the interference fringe projection technique to measure the 3D surface profile information of high pressure formed objects [19]. Chen et al. proposed an optical interference measurement system for the biomedical domain, using the Michelson interferometer and digital image processing technology to analyze the ball surface roughness of artificial joints [20]. Takaaki used non-contact optical inspection systems, such as the Twyman–Green interference and Mach–Zehnder interference methods, in the inspection structure of microlens array, and drawing the 3D surface profile of a microlens [21]. Yang et al. develop a detection system of the symmetrical microlens array especially for the cases that the sag of microlens is much longer than the wave length of light source. The proposed method is applicable to the in-line lens sag measurement of different-sized microlens array of liquid lenses in manufacturing processes [22].

The proposed system in this study adopts the principle of the Fizeau interferometer, which uses a camera to capture the interference images of a standard reference plane and a microlens array surface. Only one image is needed when analyzing the phase difference to measure the lens sag of the microlens, thus promoting the inspection speed. And the structure of the Fizeau interferometer is simpler and lower-cost than other optical interferometers, or rather easily commercialized. The inspected object can be a symmetrical or unsymmetrical microlens. For example, the interference fringe distribution of an unsymmetrical microlens is dense on one side and rare on the other, which differs from the isopycnic sides of a symmetrical type. Therefore, this study proposed an innovative algorithm: to determine the darkest and brightest points of each dark fringe and bright fringe, and then use the Bezier curve [23–25] to fit the determined points into a closed curve. These closed curves can be regarded as surface profile contour lines [26], which serve as the base for rebuilding the 3D surface profile of the microlens.

## 2. Methods of unsymmetrical microstructure measurement system

The interference fringes of microlens were obtained using the microscopic interferometry of Fizeau interferometer. The ring-shaped interference fringes contain dark fringe and bright fringe information are as shown in Fig. 1. In order to guarantee that the fringes found in the image are extremely dark fringes and extremely bright fringes, the unsymmetrical microlens is taken as an example in this study, and the extremely dark fringes and extremely bright fringes of the ring-shaped fringes would be analyzed according to the following procedures.

### 2.1. Mask operation and central position calculation of microlens

When adopting the objective lens to magnify the images of fringes, the central area of the resulted image may probably be brighter than the surrounding area. The binary result will not be good if using the traditional binary operation of a single threshold value, as it may result in numerous misjudgments. Hence, a mask operation is used to compare the gray value of the image pixel $G(x, y)$ with the mask average gray value $G_{avg}(x, y)$, to determine whether the pixel belongs to the background or the interference fringes, as shown in Eq. (1).

$$G'(x,y) = \begin{cases} 255 & if \quad G(x,y) \geq Gavg(x,y) \\ 0 & else \quad G(x,y) < Gavg(x,y) \end{cases} \tag{1}$$

$$Gavg(x,y) = \frac{\sum_{i=1}^{w}\sum_{j=1}^{h} G(i,j)}{w \times h} \tag{2}$$

where

$G'(x, y)$ is the new gray value after the mask operation, and $G(i, j)$ is the gray value of the pixel at coordinates $(i, j)$,

$G_{avg}(x, y)$ is the mask average gray value, and $w$, $h$ is the size of the mask array.

After dividing the background, the complete interference fringes and background binary image are shown as Fig. 2. Then determine the central coordinates $C(X_c, Y_c)$ of the microlens using the region filling method, as shown in the following equations and Fig. 2.

$$X_c = \frac{\sum x}{n} \tag{3}$$

$$Y_c = \frac{\sum y}{n} \tag{4}$$

where $\sum x$ and $\sum y$ are the sum of $x$-coordinates and the sum of $y$-coordinate, $n$ is the total pixels in this region.

### 2.2. Dividing bright and dark fringes and edge detection

The image is divided by tagging the ring-shaped bright and dark interference fringes individually. According to the previous mask operation, the ring-shaped interference fringes are guaranteed to be separate and mutually exclusive in binary results, only the isolated points will be removed by the concept of "eight-adjacent points". Since the brightness of every pixel may be changed after denoising, such as the low-pass filter and the

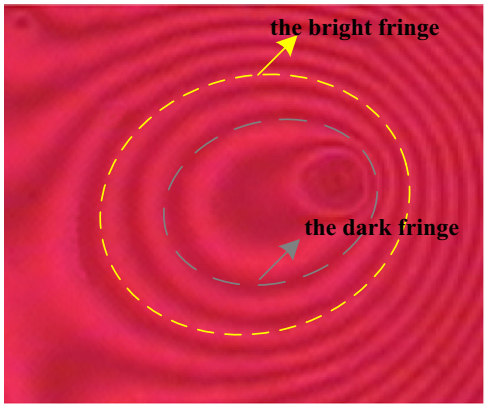


**Fig. 1.** Interference fringe image of unsymmetrical microlens.

**Fig. 2.** Result of central point.

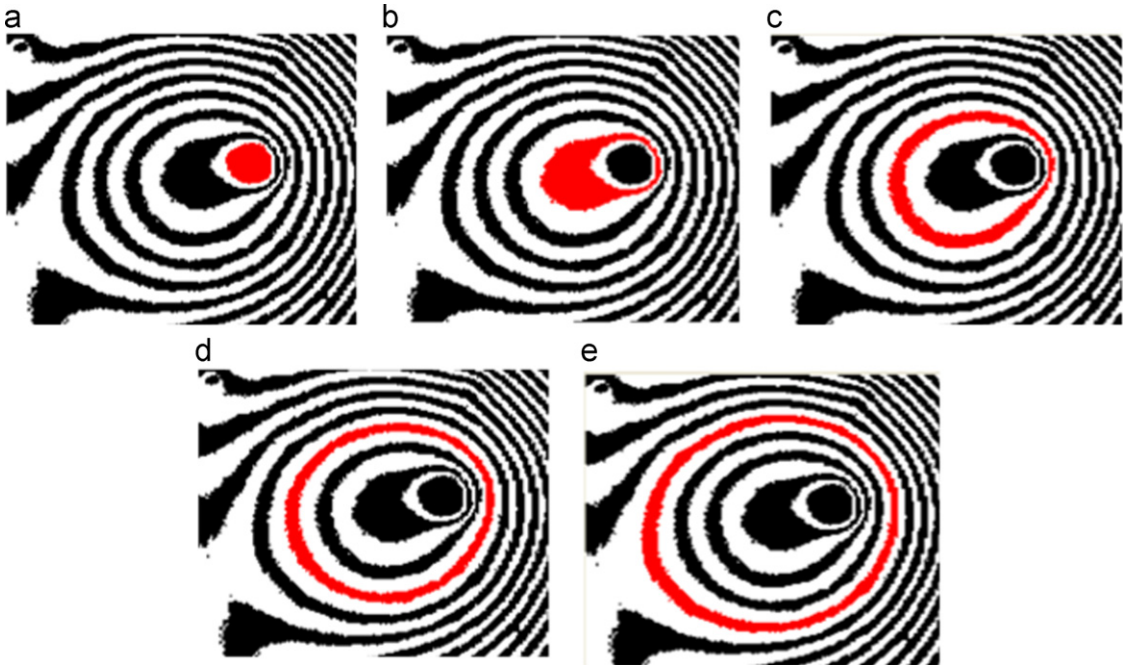


**Fig. 3.** Dark fringe division result: (a) Loop 1 (b) Loop 2 (c) Loop 3 (d) Loop 4 (e) and Loop 5.

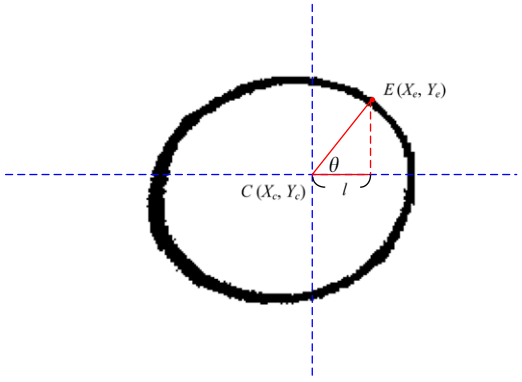


**Fig. 4.** Scan edge point coordinates of interference fringe at fixed angle $\theta$.

median filter etc., the similar operations are avoid using in this paper to promote the accuracy of the searching results and the completeness of the optical information. The division then can be completed by the "connectivity priciple" as shown in Fig. 3(a)–(e), the dark fringes of each microlens can be divided into 5 tags (5 ring-shaped interference fringes); similarly, the bright fringe can be divided into 4 tags.

The scattering points are removed from the divided single interference fringe, and then the edge point coordinates are searched using an innovative method. A ray is initiated from the central coordinates $C$ ($X_c$, $Y_c$) of the microlens to the edge of interference fringe, where each turning is at fixed angle $\theta$ for 360° scanning, as shown in Fig. 4.

The gray values of the interference fringe pixels of the ray are analyzed. If the variation in brightness of two adjacent pixels is from dark to bright, and the gradient is 255, then the dark point must be the edge point of interference fringe. The equation of this ray can be expressed as follows:

$$\begin{cases} Xe = Xc + l \\ Ye = Yc + l\tan\theta \end{cases} \quad (5)$$

where $l > 0$ and $0 \le \theta < 2\pi$.

**Fig. 5.** Result of edge detection of each dark fringe.

Therefore, according the aforesaid principle, if there are two adjacent points, $(X_c+l, Y_c+l\tan\theta)$ and $(X_c+(l+\Delta l), Y_c+(l+\Delta l)\tan\theta)$, in the binary image of interference fringe, and they meet the following equation:

$$g(X_c+(l+\Delta l),\quad Y_c+(l+\Delta l)\tan\theta) - g(X_c+l, Y_c+l\tan\theta) = 255 \quad (6)$$

where

$$g(X_c+(l+\Delta l),\quad Y_c+(l+\Delta l)\tan\theta) \quad \textit{and} \quad g(X_c+l,\quad Y_c+l\tan\theta)$$

represent the gray values of the two adjacent pixels, respectively.

$(X_c+l, Y_c+l\tan\theta)$ must be the edge point of interference fringe; the complete interference fringe edge sets can be obtained by repeating this procedure. For example, the searched result for the edge detection of the dark fringes is shown in Fig. 5.

### 2.3. Constructing the radial lines

The dark fringe is also taken as an example, where $E_1$, $E_2 \ldots E_n$ represent the edge points of every dark fringe, and their coordinate points are $(x_{e_1}, y_{e_1})$, $(x_{e_2}, y_{e_2}) \ldots (x_{e_n}, y_{e_n})$. Each edge point is connected to the central coordinate point $C$ using Eq. (5), which is a straight line equation; this connection is called radial lines. As shown in Fig. 6, $\overline{CE_1}$, $\overline{CE_2}$, $\overline{CE_3} \ldots \overline{CE_n}$ line segments represent the radial lines of connection between the edge points and center point.

Since the radial lines pass through every dark fringe, the extremely dark points of the radial lines in each interference fringe can be determined. Fig. 7 shows the schematic diagram of the radial lines passing through the outermost dark fringe, where radial line No. $n$ has $k$ pixels $R_{n1}$–$R_{nk}$, herein $g(R_{11})$, $g(R_{12}) \ldots g(R_{1k})$

represent the gray values of $k$ pixels passing through radial line $\overline{CE_1}$. Brightness is analyzed according to the gray values of $k$ pixels in order to determine the coordinate point with the minimum brightness value, i.e. the extremely dark point of this radial line. Each dark fringe is calculated in the same way using a circular method to determine the extremely dark point on each dark fringe. In a similar manner, the coordinate point with the maximum brightness value among $k$ pixels is determined to identify the extremely bright point of each bright fringe.

### 2.4. Using the Bezier curve to fit microlens profile contour lines

When the extremely bright points and the extremely dark points are determined, as there may be omitted points between these extreme points, neither the extremely bright fringe nor the extremely dark fringe are closed curves. Therefore, the "Bezier curve" algorithm is modified in this study for curve fitting [23,27], where the fitted closed curve is the microlens profile contour line, and the altitude difference is the quadrant light wavelength.

A second-order Bezier curve is used to fit the extremely bright fringes and the extremely dark fringes. The dark fringe is taken as an example, every three pixels of the extremely dark fringes is set as a group, and the extremely dark fringes are fitted with multi unit Bezier curves as shown in Fig. 8.

The unit Bezier curve is composed of $P_0$, $S$ and $P_2$, where $P_0$ is the start point of the unit Bezier curve, $P_2$ is the end point of the unit Bezier curve and $P_1$ is the control point of the unit Bezier curve. Point $L$ varies from $P_0$ to $P_1$ and describes a linear Bezier curve. The equation of this curve can be expressed as follows:

$$L(t) = (1-t)P_0 + tP_1, \quad t \in [0,1] \tag{7}$$

In a similar manner, point $R$ varies from $P_1$ to $P_2$ and also describes a linear Bezier curve. The equation of this curve can be expressed as follows:

$$R(t) = (1-t)P_1 + tP_2, \quad t \in [0,1] \tag{8}$$

Point $S(t)$ varies from $L$ to $R$ forms a second-order Bezier curve, which can be expressed as follows:

$$S(t) = (1-t)^2P_0 + 2t(1-t)P_1 + t^2P2\,, \quad t \in [0,1] \tag{9}$$

To evaluate the coordinates of the control point $P_1$, the point $S$ could be set as the highest in every unit Bezier curve, that is, the $y$ coordinate of $S$ is relatively larger than the $y$ coordinate of all the other points on the unit Bezier curve as shown in Fig. 9.

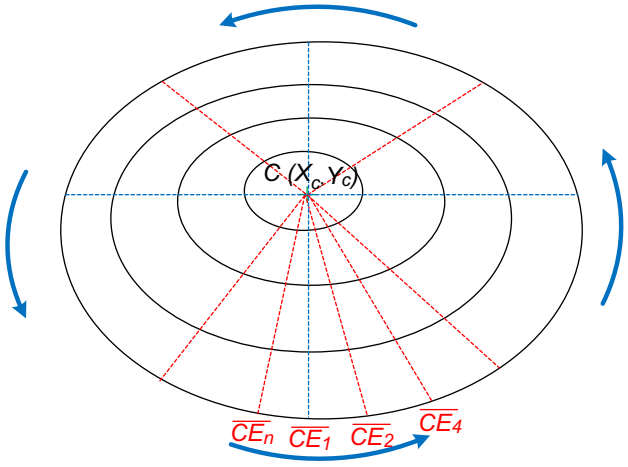


**Fig. 6.** Schematic diagram of radial lines of outermost dark fringe.

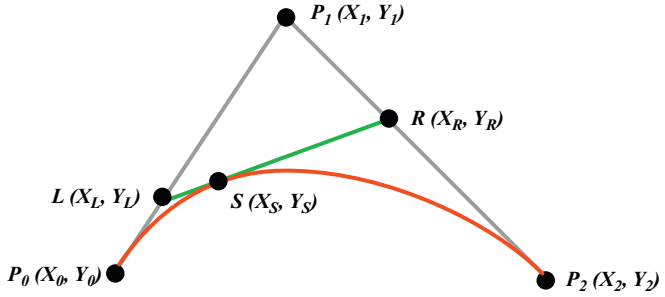


**Fig. 8.** A second-order Bezier curve is composed of $P_0$, $S$ and $P_2$.

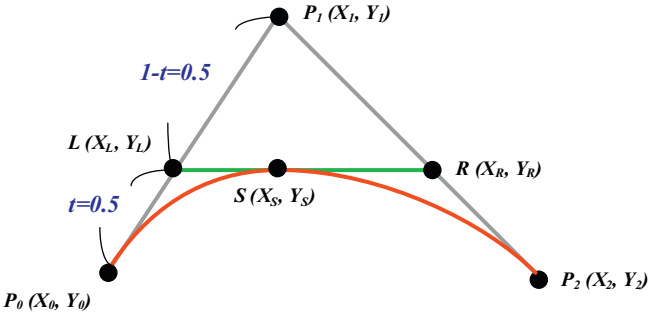


**Fig. 9.** Set the point $S$ the highest point in every unit Bezier curve to evaluate the control point $P_1$.

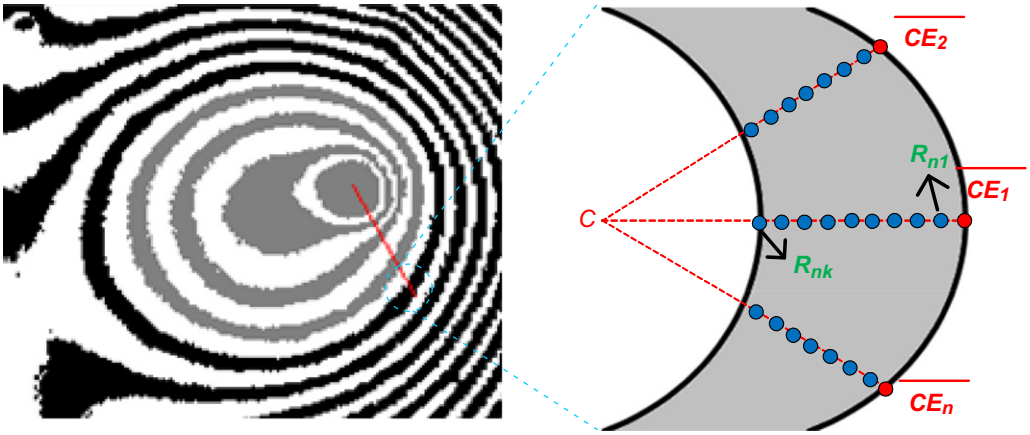


**Fig. 7.** Schematic diagram to determine the extremely dark point of radial lines.

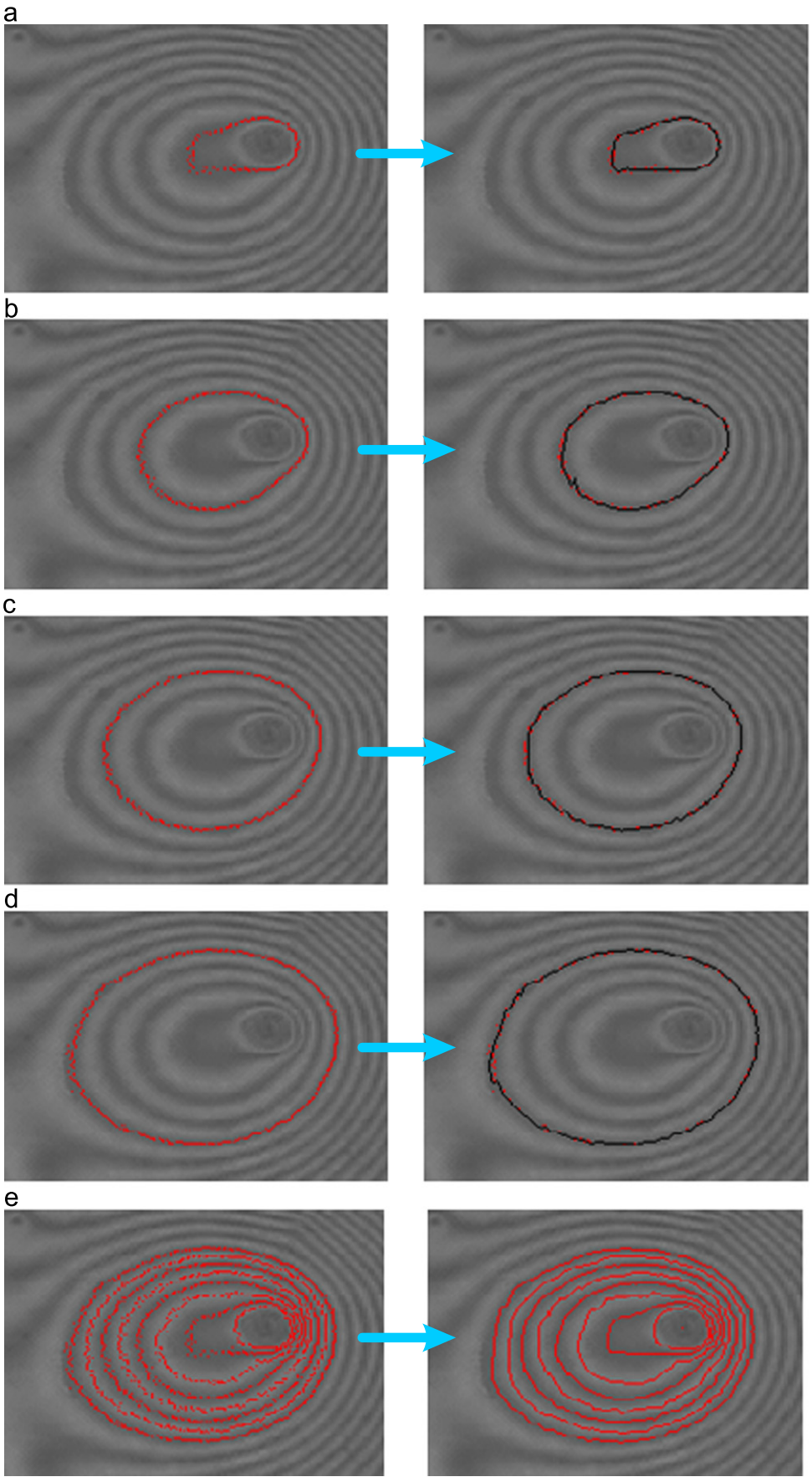


**Fig. 10.** Extremely dark fringe curve fitting result: (a) Loop 2 (b) Loop 3 (c) Loop 4. (d) Loop 5 and (e) complete microlens profile contour lines.

Since the point $S$ is the highest point in every unit Bezier curve, $\overline{LR}$ is parallel to the $\overline{P_1P_2}$, and the value of $t$ can be solved as follows:

$$\frac{1-t}{t}=\frac{t}{1-t}\Rightarrow t=0.5 \tag{10}$$

The coordinates of the control point $P_1$ then can be calculated with the given values $P_0(X_0, Y_0)$, $P_2(X_2, Y_2)$ and $t=0.5$, as shown below:

$$P1=\frac{S(t)-(1-t)^2P0-t^2P2}{2t(1-t)},\quad t=0.5 \tag{11}$$

The fitted closed curves of every extremely dark fringe and the complete microlens profile contour lines are shown in Fig. 10.

### 2.5. Rebuild three-dimensional surface profile of microlens

The phase angle of the interference fringes changes from 0° to 180°, indicating the microlens surface variation is $\lambda/4$. But the phase angles of the innermost ring and outermost ring are probably not a complete change. Hence, the phase difference of every neighboring pixel along the radial lines is calculated according to the gray value curve, and the gray value curve of the interference image can be obtained along the microlens

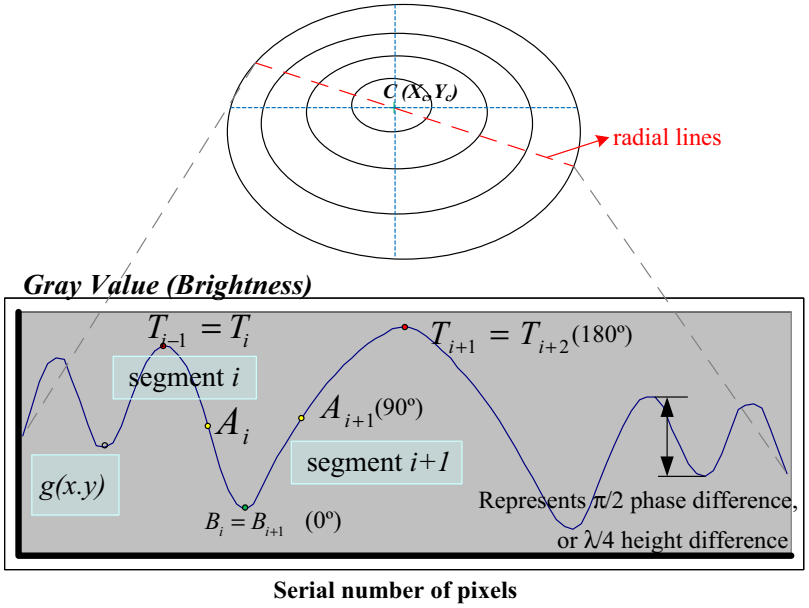


**Fig. 11.** The gray value curve of the interference image along the radial lines.

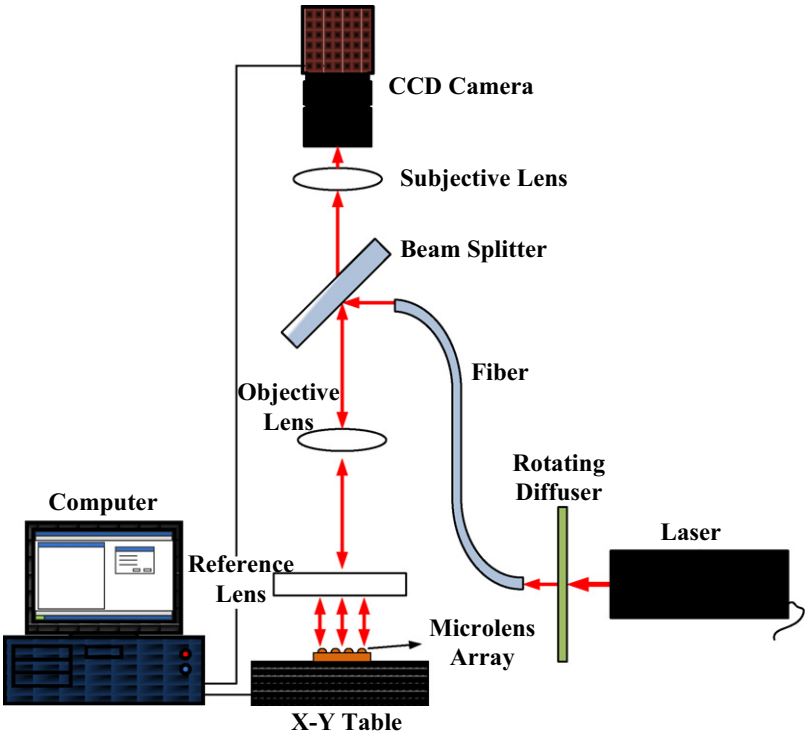


**Fig 12.** Schematic diagram of inspection system structure.

center. The variation of the brightness in this curve could be divided into the 1st segment, the 2nd segment, …, and the nth segment as shown in Fig. 11.

Find maximum value $T_i$ and minimum value $B_i$ of the brightness curve of the *ith* segment, $g(x, y)$ is brightness of pixel $(x, y)$ *on* the *ith* segment of brightness curve.

Let $\Delta_i$ be the brightness variation of the *ith* segment,

$$\Delta_i = |T_i - B_i| \tag{12}$$

Let $A_i$ be the brightness of the *ith* segment at a phase angle of 90°,

$$A_i = B_i + \frac{\Delta_i}{2} \tag{13}$$

The phase angle difference $\delta\theta(x, y)$ between the point $(x, y)$ and $(x+1, y)$ in the *ith* segment can be calculated as follows:

$$d\theta(x,y) = \cos^{-1}\left[2\frac{g(x,y)-A_i}{\Delta_i}\right] - \cos^{-1}\left[2\frac{g(x+1,y)-A_i}{\Delta_i}\right] \tag{14}$$

where $g(x, y)$, $g(x+1, y)$ are the gray value of the point $(x, y)$ and $(x+1, y)$.

Suppose the noise of background is smooth and uniformly distributed in the captured image, the noise of background can be eliminated by the subtraction in the denominator $g(x, y)-A_i$ and $g(x+1,y)-A_i$. Hence, the phase angle of the innermost and outermost interference fringe then can be calculated by the extrapolation method without the influences of background noise.

Then the corresponding microlens surface altitude difference $\delta l(x)$ between point $(x, y)$ and $(x+1, y)$ in this segment can be obtained according to the following equation [28]:

$$dl(x) = \left[\frac{\lambda}{4\pi}\right] \left|\cos^{-1}\left[2\frac{g(x,y)-A_i}{\Delta_i}\right] - \cos^{-1}\left[2\frac{g(x+1,y)-A_i}{\Delta_i}\right]\right| \tag{15}$$

Let the segment where center circle $(x_c y_c)$ lies be the nth segment, the lens sag is the sum of microlens surface altitude difference from the 1st segment to the segment where the microlens center $(x_c y_c)$ lies and could be obtained as following $(\Delta l)$:

$$\Delta l = \sum_{1}^{x_c} \delta l(x) \tag{16}$$

## 3. Experimental results and discussion

A non-contact AOI system is developed in this study to inspect the 3D surface profile of microstructures, especially for the unsymmetrical type. Fig. 12 shows the automatic inspection system for the 3D surface profile of a microlens, and the flow chart of microlens in-line inspection is shown as Fig. 13. The speckle noise arising from the laser beam was eliminated by a rotating diffuser, thus making the captured image clearer. The laser beam was transmitted through the fiber into the microscope set, the 20× objective lens, 2× Adapter, Navitar Manual Zoom Lens, and CCD camera form an imaging module, under which there was an XY-Table for precision positioning. The microlens sample was placed on the XY-Table, and an optical flat was placed on the microlens sample as the reference plane for the interferometer. The above-mentioned equipment was mounted on a vibration-proof platform, and the light path of the micro-interferometer was constructed to form an AOI system for the microlens.

There were two microstructure samples A and B inspected in this study, where A is a symmetrical microlens array with a lens size of 110 μm × 110 μm, and B is an unsymmetrical microlens array with a lens size of 200 μm × 165 μm. The lens sags and apertures differ, as they were constructed through different processes. To verify the accuracy of the proposed system, the ET3000 surface profiler developed by KOSAKA Company is used to inspect the lens sag of the above same samples. However, the contact profilometry is not suitable for the in-line inspection of microlens array. Since the ET3000 surface profiler uses the probe

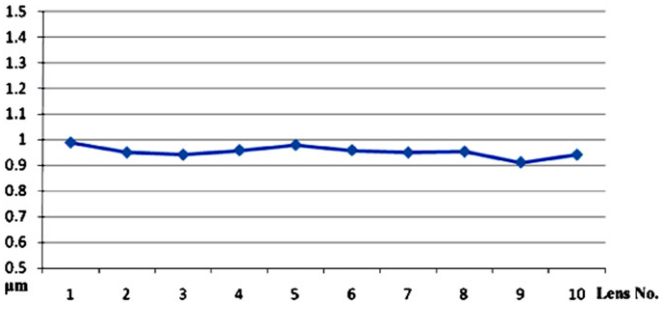


**Fig. 14.** Curve diagram of lens sag measurement of sample A obtained by this system.

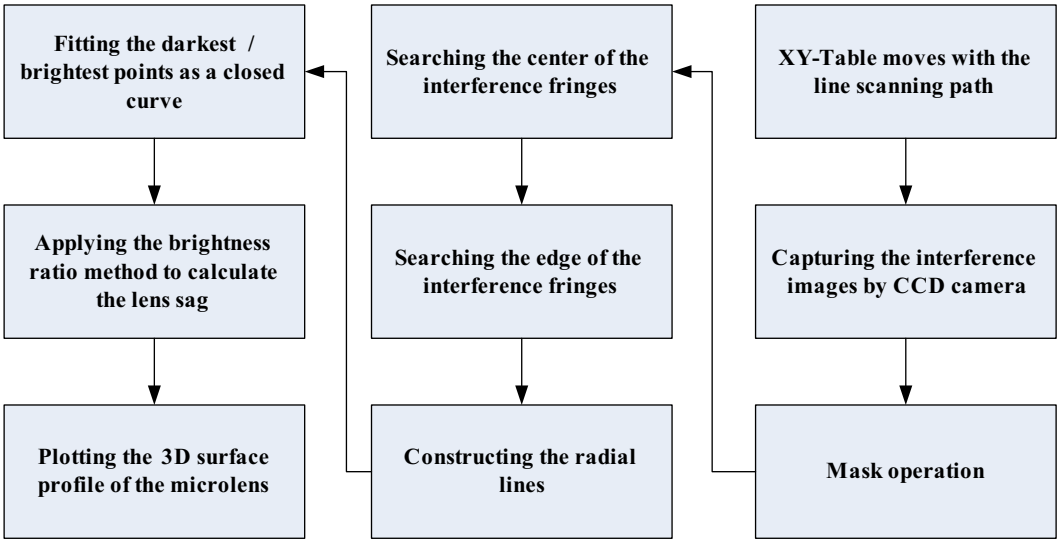


**Fig. 13.** The flow chart of microlens in-line inspection.

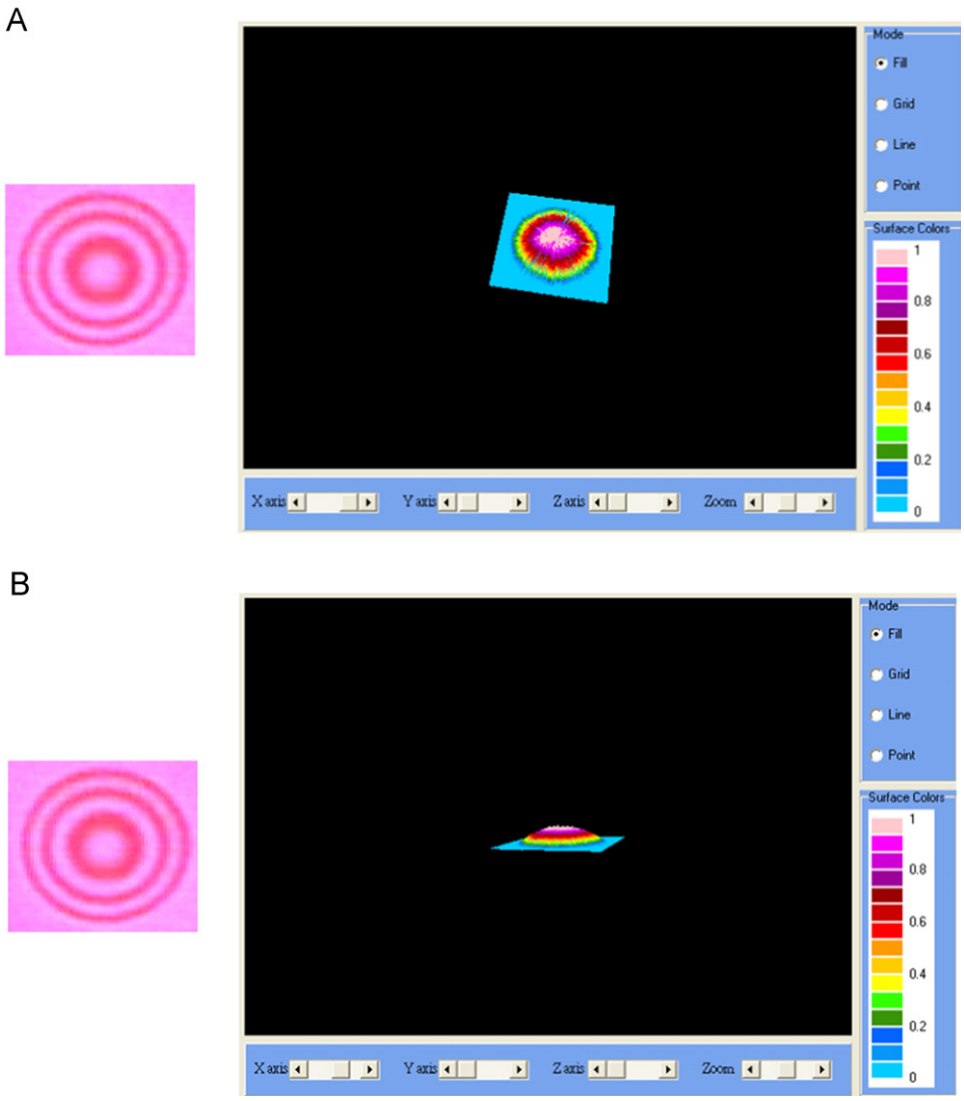


**Fig. 15.** (A) Sample A: top view of 3D surface profile of symmetrical microlens and (B) sample A: side view of 3D surface profile of symmetrical microlens.

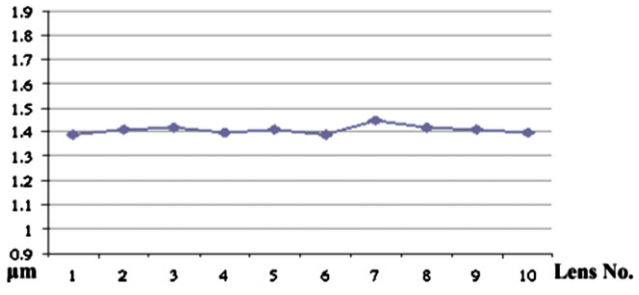


**Fig. 16.** Curve diagram of lens sag measurement of sample B obtained by this system.

to contact the surface of microlenses, and the lens sag is obtained through the vertical displacement of the contact probe, which may slightly scratch the microlenses as they are very fragile.

First, the sample A symmetrical microlens array was measured, as shown in Fig. 14, and 10 microlenses were randomly selected for measurement by this system. The Lens Sag measurement result was 0.94–0.98 μm, ET-3000 surface profiler measurement result was 0.95–0.96 μm, and the difference between these results was less than 0.02 μm. In addition, when the edge points of the ring-shaped interference fringes of microlens were determined, the 3D surface profile of the microlens could be rebuilt using the radial lines formed from the connection between the edge points and central position. Fig. 15(A) is the top view of the rebuilt 3D surface profile of the symmetrical microlens, and Fig. 15(B) is the side view.

Sample B of the unsymmetrical microlens was measured, as shown in Fig. 16. The Lens Sag measurement result was 1.39–1.45 μm, ET-3000 surface profiler measurement result was 1.42–1.43 μm, and the difference between them is less than 0.04 μm. The 3D surface profile was rebuilt according to the aforesaid principle. Fig. 17(A) is the top view of the rebuilt 3D surface profile of unsymmetrical microlens, and Fig. 17(B) is the side view.

The Lens Sag measurement results, as obtained by this system and the ET-3000 surface profiler, are as shown in Table 1. As seen, the difference between two systems was less than 0.04 μm, suggesting that 3% lateral accuracy can be achieved by the proposed system, and the proposed system has the advantage of non-contact inspection for avoiding damage to the surface structure of the analyte. Moreover, the inspection speed of the proposed system is fast since the average processing time of measuring a microlens is less than or equal to 0.5 s, and the cost is relatively reduced.

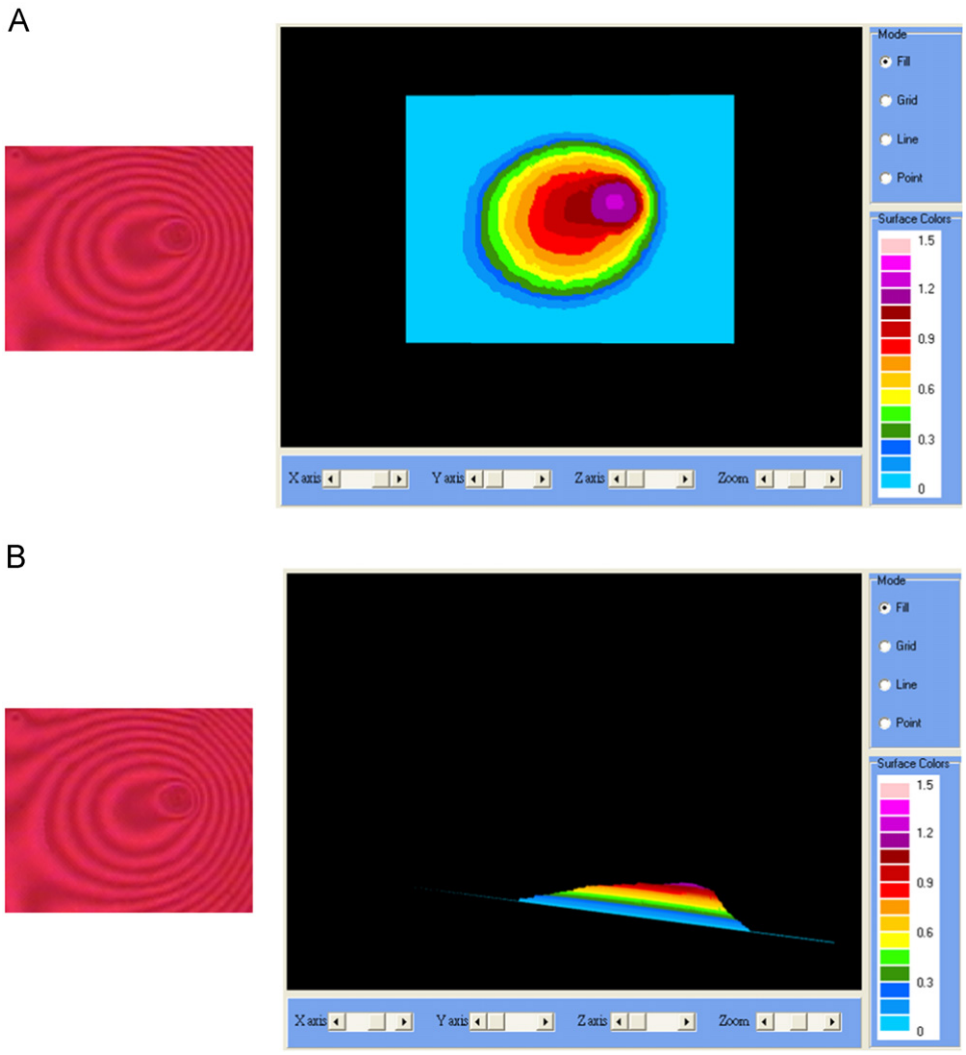


**Fig. 17.** (A) Sample B: top view of 3D surface profile of unsymmetrical microlens and (B) sample B: side view of 3D surface profile of unsymmetrical microlens.

**Table 1**
Comparison of measurement results by this system and ET3000 surface profiler.

| Inspection item (μm) | This system (μm) | ET3000 (μm) | Difference (μm) |
|---|---|---|---|
| Lens Sag of sample A | 0.94–0.98 | 0.95–0.96 | ≤0.02 |
| Lens Sag of sample B | 1.39–1.45 | 1.42–1.43 | ≤0.04 |

## 4. Conclusions

The interferometric AOI system for the 3D surface profile of an unsymmetrical microstructure consists of an XY-Table, an optical imaging module, an optical interference module, and software controls. The XY-Table controls the longitudinal and transverse translation of the entire inspection system, and is able to individually inspect the lenses. The CCD camera captures the interference image of the microlens, the noise is first removed from the image by mask operation, and then, the central position is searched using the region filling method. Afterward, the 3D surface profile of unsymmetrical and symmetrical microlens are rebuilt using the contour line surface profile method, and the edge point coordinates of the ring-shaped interference fringes are individually determined through image processing and computer graphics. Each edge point of the dark and bright fringes can be connected to the center to form radial lines, and the coordinates of the interference fringe's extreme points on the radial lines can be determined. Since these extremely bright points and extremely dark points are not always a closed curve, the Bezier curve algorithm is introduced for curve fitting these points, which is the key innovation of this paper. Finally, the 3D surface profile of a microlens can be successfully rebuilt using the phase difference between the fringes. In addition, this system has the advantage of non-contact measurement, which does not require a metal coating to form a reflective layer for measurement, thus, avoiding the destruction of the surface structure of samples. Furthermore, the 3D surface profile of the microlens to be measured can be rebuilt, and as only one image is taken each time, the inspection process is rapid.

## Acknowledgment

This work was sponsored by the National Science Council under Grant no. NSC 100-2221-E-009-024 and NSC 101-2221-E-035-039-MY2.

## References

[1] Rotich SK, Smith JG, Evans AGR, Brunnschweiler A. Micromachined thin solar cells with a novel light trapping scheme. J Micromech Microengineer 1998;8(2):134–7.

[2] Ezell B. Making microlens backlights grow up. Inf Disp 2001;5:21–6.
[3] Hartmann DM, Reiley DJ, Esener SC. Microlenses self-aligned to optical fibers fabricated using the hydrophobic effect. IEEE Photonics Technol Lett 2001;13(10):1088–90.
[4] MacFarlane DL, Narayan V, Tatum JA, Cox WR, Chen T, Hayes DJ. Microjet fabrication of microlens arrays. IEEE Photonics Technol Lett 1994;6(9): 1112–4.
[5] Lin CS, Chen CT, Wei TC, Chen WL, Chang CC. A positioning model of a two CCD camera coordinate system with an alternate-four-matrixlook-up table algorithm. Opt Lasers Eng 2010;48(12):1193–9.
[6] Lin CS, Lin CH, Lin CC, Yeh MS. Three-dimensional profile measurement of small lens using subpixel localization with color grating. Optik 2010;121(23): 2122–7.
[7] Lin CS, Wei TC, Lu AT, Hung SS, Chen WL, Chang CC. A rehabilitation training system with double-CCD camera and automatic spatial positioning technique. Opt Lasers Eng 2011;49(3):457–64.
[8] Lin CS, Lin CH, Chen DC, Tien CL, Yeh MS. Measurement method of three-dimensional profiles of small lens with gratings projection and a flexible compensation system. Expert Syst Appl 2011;38:6232–8.
[9] Lin CS, Chen CT, Shei HJ, Lay YL, Chiu CC. Development of a body motion interactive System with a weight voting mechanism and computer vision technology. Opt Laser Technol 2012;44(6):1934–41.
[10] Su D, Li X. Fractionized calibration of the sample stage used in an AFM-probe mechanical testing system. Opt Lasers Eng 2010;48(11):1076–81.
[11] Delobelle B, Courvoisier F, Delobelle P. Morphology study of femtosecond laser nano-structured borosilicate glass using atomic force microscopy and scanning electron microscopy. Opt Lasers Eng 2010;48(5):616–25.
[12] Poon CY, Bhushan B. Comparison of surface roughness measurements by stylus profiler, AFM and non-contact optical profiler. Wear 1995;190(1): 76–88.
[13] Badami VG, Smith ST, Raja J, Hocken RJ. A portable three-dimensional stylus profile measuring instrument. Precis Eng 1996;18(2–3):147–56.
[14] Poole I, Lloyd GE. Alternative SEM techniques for observing pyritised fossil material. Rev Palaeobot Palynol 2000;112(4):287–95.
[15] Guise O, Strom C, Preschilla N. STEM-in-SEM method for morphology analysis of polymer systems. Polymer 2011;52(5):1278–85.
[16] Yamamoto A, Yamaguchi I. Surface profilometry by wavelength scanning Fizeau interferometer. Opt Laser Technol 2000;32(4):261–6.
[17] Charriere F, Kuhn J, Colomb T, Montfort F, Cuche E, Emery Y. Characterization of microlenses by digital holographic microscopy. Appl Opt 2006;45(5): 829–35.
[18] Anna T, Shakher C, Mehta DS. Three-dimensional shape measurement of microlens arrays using full-field swept source optical coherence tomography. Opt Lasers Eng 2010;48(11):1145–51.
[19] Quan C, Tay CJ, Shang HM. Fringe projection technique for the 3-D shape measurement of a hydroformed shell. J Mater Process Technol 1999;89-90(19):88–91.
[20] Chen X, Grattan KTV, Dooley RL. Optically interferometric roughness measurements for spherical surfaces by processing two microscopic interferograms. Measurement 2002;32(2):109–15.
[21] Miyashita T. Standardization for microlenses and microlens arrays. Jpn J Appl Phys 2007;46(8):5391–6.
[22] Yang SW, Lin CS, Fu SH, Yeh MS, Tsou C, Lai TH. Lens Sag measurement of microlens array using optical interferometric microscope. Opt Commun 2012;285(6):1066–74.
[23] Schneider PJ. An algorithm automatically fitting digitized curves, Graphics Gems. San Diego: CA: Academic Press; 1990 pp. 612–626.
[24] Chang HH, Yan H. Vectorization of hand-drawn image using piecewise cubic Bezier curves fitting. Patt Recog 1998;31(11):1747–55.
[25] Cinque L, Levialdi S, Malizia A. Shape description using cubic polynomial Bezier curves. Pattern Recognition Lett 1998;19:821–8.
[26] Yang X, Yu Q, Fu S. Determination of skeleton and sign map for phase obtaining from a single ESPI image. Opt Commun 2009;282(12):2301–6.
[27] Bezier P. Mathematical and practical possibilities of UNISURF, computer aided geometric design. New York: NY: Academic Press; 1974 pp. 317–326.
[28] Lin CS, Loh GH, Fu SH, Yang SW, Chang HK, Yeh MS. An automatic evaluation method for the surface profile of the microlens array using an optical interferometric microscope. Meas Sci Technol 2010;21(10):1–10.